Application of Sentinel-1 Data for Classifying Croplands Using Google Earth Engine

Mirelva, P. R.[1] and Nagasawa, R.[2]
[1]The United Graduate School of Agricultural Sciences, Tottori University, 4-101 Koyama Minami, Tottori, 680-8553, Japan, E-mail: prima.rizky.m@gmail.com
[2]Faculty of Agriculture, Tottori University Tottori, Japan, E-mail: nagasawa@muses.tottori-u.ac.jp

Abstract

The agricultural sector is an important source of national income in many tropical countries, including Indonesia. Monitoring agricultural is essential to support the agricultural activities. However, these countries have tropical monsoon climate with heavy amounts of rainfall. Therefore, temporal monitoring using microwave remote sensing is beneficial to overcome the heavy cloud coverage, which is often an obstacle for applying optical remote sensing. Recently, the growing trend of cloud-based geospatial platforms, such as Google Earth Engine (GEE), provides processing tools and cloud storage for remote sensing data without high specification hardware. In this study, Sentinel-1 synthetic aperture radar (SAR) sensor data from 2017 and supplementary Sentinel-2 optical sensor data was obtained and processed in GEE to identify two types of cropping patterns in paddy fields and to classify agricultural croplands. Four types of polarization combination datasets and a random forest classifier set with number of trees to be 25 and 50 were used for the classification process. The classification results show that the VH, VV, and the subtraction of VH and VV polarization with a random forest of 50 trees was achieved with 76.88% of overall accuracy and the kappa value equaled 0.728. The random forest with 50 trees significantly increased the classification accuracy of the dataset with fewer band compositions. The Sentinel-1 images are believed to be satisfactorily accurate enough for agricultural cropland classification and are sufficient for identifying the two cropping patterns in paddy fields.

1. Introduction

The agricultural sector is important for the Indonesian economy. According to the Indonesian statistics, the agricultural sectors contributed approximately 9.9% of Indonesia's gross domestic product in 2017. Many people living in rural areas depend on agricultural activities for their main source of income. One of the prominent agricultural areas on Java Island is found in the upper Solo basin of the Central Java Province. This area has rich and fertile soil with enough water discharge to make agricultural activities viable. However, the dense populations of Java and its uneven road structure force the agricultural fields to be small in size and complex in shape. The agricultural parcels size in Indonesia is around 0.3 Ha per household (Agus and Manikmas, 2003). Most of the farmers in this area manage and cultivate croplands depending on the meteorological and topographic conditions. It is common to have paddy fields in flat areas and upland fields in hilly areas. Paddy is the main crop for this agricultural sector as it is consumed by the majority of Indonesian people and requires an abundant amount of water in the early stage of cultivation, which is complemented by the heavy rainfalls. Beyond rainfall, the water for paddy cultivation is also sourced through irrigation. The intercropping method is often practiced to increase the farmers' income. Therefore, it is common to find different cropping patterns in these agricultural fields throughout the year.

The Indonesian government has monitored agricultural croplands using direct field survey and remote sensing technology. A direct field survey is time consuming and requires surveyors. Satellite remote sensing consists of optical sensor data and synthetic aperture radar (SAR) data and provides wide range spatial and temporal data. Optical remote sensing is susceptible to the atmospheric conditions, especially during the tropical monsoon season. The SAR satellite offers active remote sensing is capable to penetrate the atmospheric conditions and provides cloud cover free data.

Recently, satellite remote sensing data has drastically improved in terms of temporal and spatial resolution used to produce the large satellite images. Developing countries or communities with limited budgets could have difficulty accessing these satellite images. However, the advanced

Online ISSN 2673-0014/

technology of cloud-based computing provides an efficient and low cost alternative for processing these images. The Google Earth Engine (GEE) is one of the cloud-based geospatial platforms that provide numerous collections of geospatial datasets and algorithms to process the satellite images. It offers flexibility to the users for conducting research related to satellite images and geospatial data. Users are able to process these datasets as long as an internet connection is available. In recent years, GEE has been used for many remote sensing applications, such as land cover change (Sidhu et al., 2018), cropland mapping (Xiong et al., 2017), and crop classification analysis using huge amounts of multi-temporal data, (Shelestov et al., 2017) because of its simplicity and user friendly interface.

There are several types of SAR wavelengths used in microwave remote sensing, such as X-band (2.5–4 cm), C-band (4–8 cm), and L-band (15–30 cm). Besides penetration through cloud, the SAR images could detect the moisture condition as well as the canopy or surface structure. Therefore, SAR data is advantageous for monitoring agriculture even in tropical areas (Nelson et al., 2014). One of the SAR satellite images provided by GEE is the C-band SAR of Sentinel-1. The C-band wavelength is shorter than the L-band wavelength, and the C-band wavelength could not penetrate deeper than the L-band wavelength. Sentinel-1 data has been applied in several studies for hydrological dynamic in wetland area (Cazals et al., 2016) as well as for agricultural applications, such as mapping rice planted areas (Clauss et al., 2017 and Tian et al., 2018), temporal behavior of crops (Veloso et al., 2017), and rice growth monitoring (Torbick et al., 2017).

The L-band SAR, ALOS/PALSAR, is often used for agricultural cropland classification, such as paddy field identification (Zhang et al., 2011), and the classification of abandoned paddy fields (Yusoff et al., 2016). The L-band SAR, ALOS/PALSAR-2, is used for classifying agricultural croplands (Mirelva and Nagasawa, 2018). However, the L-band SAR has a longer revisit time than the C-band SAR. This creates the need to consider the agricultural fields' cropping patterns before selecting the satellite images to fit the cropping pattern of agricultural fields. Sentinel-1 offers high temporal images that are useful for understanding the cropping pattern, especially in complex agriculture croplands with uncertain cropping patterns.

Recently, Ghazaryan et al., (2018) reported the effectiveness of Sentinel-1 and GEE for identifying the cereal cropping system in one of regions in continental Europe. However, few studies have used Sentinel-1 and GEE in the Asian region, specifically the areas with a tropical monsoon climate. In the present study, the combination of Sentinel-1 data and GEE was implemented to identify small, mixed agricultural crop fields in the tropical Asian region. The complex agricultural cropland in the Central Java Province (an area of approximately 112 km^2) was selected because of its irregular cropping patterns, various types of cropland, and the other surrounding land covers, such as woodland and settlement. This study aimed to understand the characteristics of Sentinel-1 when classifying two cropping patterns of paddy fields and other land use or land cover types, as well as the classification performed in GEE.

2. Materials and Methods

2.1 Study Area

The study area is located on the southeastern slopes of the Merapi volcano in the Klaten Regency of Central Java in Indonesia. The area is in the boundary of the following coordinates: 7º 37′ 10.7″-7º 42′ 56.8″ South Latitude and 110º 29′ 31.89″-110º 35′ 17.02″ East Longitude. The study area coverage appears as a red square on the map and the Pleiades image, taken in 2015, was used for information on the land use and the land cover in the study area as can be seen in Figure 1. The altitude varies from 200-600 meters above sea level.

The Merapi volcano is one of the most active volcanoes on the island of Java. Therefore, the soil is nutrient-rich which is beneficial for agricultural activities. Most people who live in this area work as farmers or sharecroppers and depend on agricultural production for their livelihood. In general, land usage can be divided into northern and southern sections. The northern area has a higher altitude and is mainly covered by settlement, woodland, and upland fields. The southern area is relatively flat and is generally covered by settlement and agricultural fields, such as paddy and tobacco fields.

2.2 Datasets

The study materials consisted of 56 satellite images of dual polarization of C-band SAR Sentinel-1 taken in 2017, the 49 satellite optical images of Sentinel-2 collected in 2017 and the Pleiades image taken on August 26, 2015. Only the Sentinel-1 and Sentinel-2 were acquired from the GEE data collection. Sentinel-1 has two polarization types, VH and VV polarization. VH polarization transmits microwaves in a vertical direction and receives scatter from the surface in a horizontal direction. VV polarization transmits and receives the microwaves in a vertical direction. The Sentinel-1 and Sentinel-2 have a 10 meter resolution and the Pleiades image has 0.6

meter resolution. Table 1 shows the availability of acquisition dates for both Sentinel-1 and Sentinel-2.

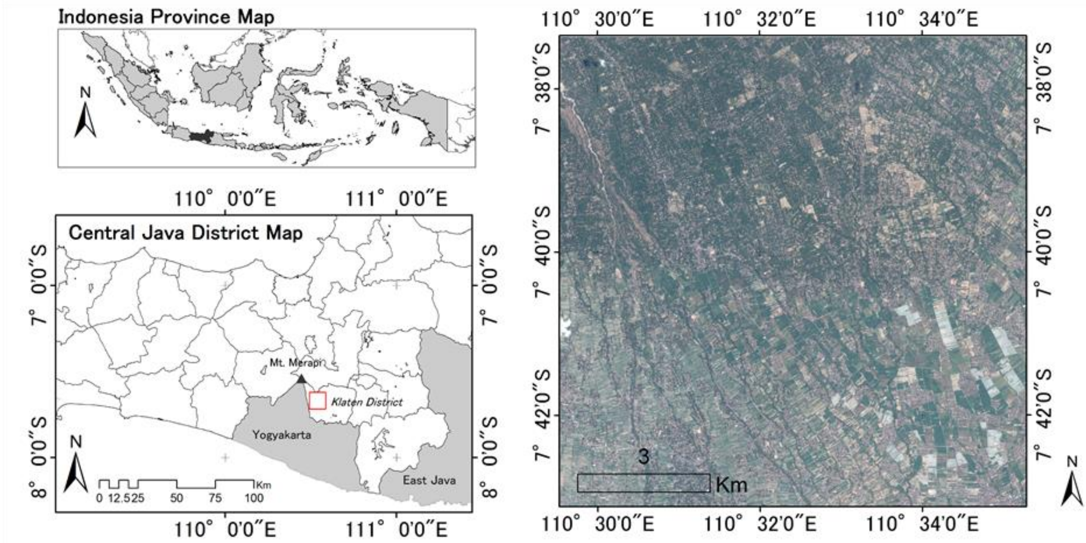

Figure 1: Study area coverage with Pleiades image taken on 2015

Table 1: Sentinel-1 and Sentinel-2 acquisition date

	Date of acquisition			**Date of acquisition**	
Month	**Sentinel-1**	**Sentinel-2**	**Month**	**Sentinel-1**	**Sentinel-2**
January	3, 27	9, 19, 29	July	2, 6, 14, 18, 26, 30	13, 18, 28
February	8, 20, 24	8, 18, 28	August	7, 11, 19, 23, 31	2, 7, 12, 17, 22, 27
March	4, 8, 16, 20, 28	10, 20	September	4,12, 16, 24, 28	1, 6, 11, 16, 21
April	1, 9, 13, 21, 25	9, 19, 29	October	6, 10, 18, 22, 30	1, 6, 11, 21, 26, 31
May	3, 7, 15, 19, 27, 31	9, 19, 29	November	3, 11, 15, 23, 27	5, 10, 15, 20, 25, 30
June	8, 12, 20, 24	8, 18, 28	December	5, 9, 17, 21, 29	5,10, 15,20, 25, 30

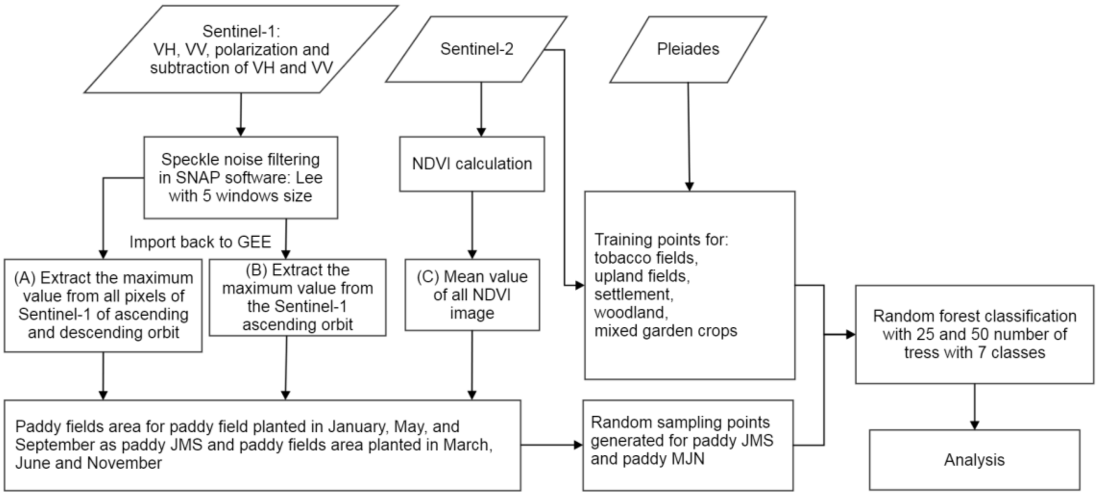

Figure 2: Overall framework for cropland classifying in GEE

2.3 Methodology

The methodology can be separated into two parts, pre-processing and the classification process. The Sentinel-1 was downloaded and processed in GEE, except for the speckle noise filtering process which was processed in Sentinel Application Platform (SNAP) software (SNAP software). The classification process was done in GEE by using the random forest classifier. The methodology details are described in the following sections and the framework of methodology can be found in Figure 2.

2.3.1 Data pre-processing

GEE data collections provide satellite remote sensing data, including Sentinel data. The Sentinel-1 data used SAR system which capable to penetrate cloud coverage. In addition, it has high temporal data which is useful to be used for monitoring agricultural condition in Indonesia. In GEE, to get one year of data, the Sentinel-1 was filtered by setting a boundary area similar to the study area and the date range from January 1 to December 31, 2017. The Sentinel-1 data from GEE data collection was already pre-processed using the Sentinel-1 Toolbox, a software for SAR satellite data processing from ESA (European Space Agency). The pre-processing steps are thermal noise removal, radiometric calibration, and terrain correction by using SRTM 30 or ASTER DEM. The ASTER DEM is used for the area located above 60 degrees of latitude, or when the SRTM is unavailable. Thus the SRTM was used in this study. However, the speckle noise reduction process was not yet performed because GEE has no algorithm to execute this process. The speckle noise reduction is important because the radar data is often affected by the coherent summation of the signals that scattered from ground (Saxena and Rathore, 2013). Therefore, the speckle noise reduction in Sentinel-1 was processed outside the GEE environment by using the SNAP software.

In order to reduce the speckle noise using SNAP software, the data collection of Sentinel-1 was clipped using the boundary of the study area and downloaded from GEE to the user's local drive. Then, a Lee filter with a 5 window size was used to reduce the speckle noise in the study area. After the speckle noise reduction, the VH and VV polarizations images were stacked and re-uploaded to the GEE as an asset for the further process. Besides the Sentinel-1 data, the subtraction between VH and VV polarization (VH-VV) for each image were also calculated. The speckle noise process was applied to the subtraction of VH and VV polarization with similar steps.

Sentinel-2 images are often affected by clouds; therefore, the cloud removal process for Sentinel-2 was processed in GEE. In general, the cloud removal process consists of cloud and shadow removal. Cirrus clouds were removed by subtracting the bands in each image with the cirrus band or the tenth band of Sentinel-2. The cloud area with a greater thickness than cirrus was selected with the rule condition if the reflectance value in red band, green band, and blue band are greater than 1700. Meanwhile, the shadow was removed based on the calculation of green (B3), blue (B2), and red edge (B8A) bands. The area identified as a shadow if the red edge reflectance value is between 900 and 1800, and the division of blue and green band is greater than 1.2. These calculations were modified from the automatic cloud and shadow detection for optical satellite imagery (Parmes et al., 2017). Then, the normalized difference vegetation index (NDVI) was calculated from the ratio of the near infrared band (B8) and the red band (B4).

2.3.2 Classification process

The GEE provides several types of supervised and unsupervised classification algorithms. In this study, the supervised classification named "random forest" was chosen as the classifier. The random forest algorithm, in simple terms, can be defined as a forest made of several decision or predictor trees. Each tree depends on the value of the random sample independently, with equal distribution for the entire tree in the forest (Breiman, 2001). The study area is divided into classes named upland fields, paddy, tobacco fields, settlement, woodland, and mixed garden crops. The training and accuracy assessment points for settlement, woodland, upland fields and mixed garden crops classes were selected based on the Pleiades image, with the assumption that the land use and land covers change of these classes was minimum and could be neglected. The class of tobacco fields was selected from the Sentinel-2 optical images. Meanwhile, the sample points and accuracy assessment points for the paddy fields were selected based on Sentinel-1 data.

The field survey conducted on August 2017 presented the paddy fields area in diverse stages. It was common to have some area in the early cultivation stage and the other area in the harvest stage. The steps for selecting the sample point for these paddy classes were as follows:

(a) The woodland in the northern area and settlement areas are masked out. The average NDVI of Sentinel-2 in 2017 is calculated and a value greater than 0.63 is used as a woodland mask. The settlement mask for the average value of NDVI is less than 0.38, and the average VV band is greater than -3.8 dB. On the other hand, the slope area is masked out with the value less than -9 dB from the maximum VV polarization in one year.

(b) The early stages for paddy fields, like transplanting, are crucial for detecting paddies using the SAR remote sensing, because this stage requires a lot of water. The 39 points from the transplanting stage during the field survey on

August 2017 was selected for calculating the average value of the backscatter coefficient. Thus, in this study, the area identified as paddy if the backscatter coefficient of each image is between -31 to -17.4852 dB (from the average value calculation). This step changes images into Boolean data, with 0 as false and 1 as true (fulfill the rule conditions).

(c) Sentinel-1 images were divided into six groups according to the image acquisition month: January to February as (a), March to April as (b), May to June as (c), July to August as (d), September to October as (e), and November to December as (f). The total value was changed into Boolean values by applying a rule greater than 1 for the January to February group, and greater than 2 for the other groups. These rules are generated because the image acquisition in January and February are less than in other months.

(d) The paddy fields were often cultivated two or three times a year. Therefore, paddy fields were separated into two types, paddy planted in January, May, or September, and named Paddy-JMS, and paddy planted in March, July, and November, named Paddy-MJN class. The area with the value equaling 2 or 3 from the total of (a), (c), and (e) groups indicate Paddy-JMS, and the area with the value equaling 2 or 3 from the total of (b), (d) and (f) groups indicate Paddy-MJN. The value equaling 1 indicates that the area was rarely cultivated as paddy fields and more likely to contain other croplands, such as maize, cassava, or other vegetable crops. Therefore, the area equaling 1 was omitted.

(e) Following that, the images of the Paddy-JMS and Paddy-MJN area were converted into vector polygons. Both the vector polygons were used to generate 90 random points.

The classification was run in GEE with the proportion around 70% sample points and 30% accuracy assessment points for all classes, which is described on Table 2. The random forest classifier was set with two numbers of trees equal to 25 and 50. There are four sets combination of Sentinel-1 polarization images (VH and VV) and the VH-VV polarization used for classifications. Table 3 describes the detail of four sets of polarization combinations for the classification. Thus, there were eight classifications generated in this study.

3. Results and Discussion

3.1 Sentinel-1 and Sentinel-2 Data Pre-Processing

Figure 3 shows the Sentinel-1 image before and after the speckle filtering process for an image taken on January 3, 2017. The RGB in Figure 3 is set with VV, VH, and VH-VV polarizations band composite to analyze the effect of speckle filtering. The backscatter coefficient became lower and the salt-pepper noise was decreased after the speckle filtering process, as can be seen in Figure 3(b).

Table 2: Detail description of sample and accuracy assessment points

Class Name	Sample Points	Accuracy Assessment Points	Total Points
Upland fields	73	31	104
Paddy-JMS	62	28	90
Paddy-MJN	63	27	90
Tobacco fields	40	16	56
Woodland	70	28	98
Settlement	72	29	101
Mixed garden crops	65	27	92
Total Points	445	186	631

Table 3: Polarization combination for the classification process

Polarization Combination Name		Description of Polarization Combination	Number of Images
25	50		
A_25	A_50	VH and VV polarization	112
B_25	B_50	VH, VV, subtraction of VH and VV	168
C_25	C_50	VH, VV, subtraction of VH and VV taken on January to February, May to June and September to October	75
D_25	D_50	VH, VV, subtraction of VH and VV taken on March to April,	91

		July to August and November to December	

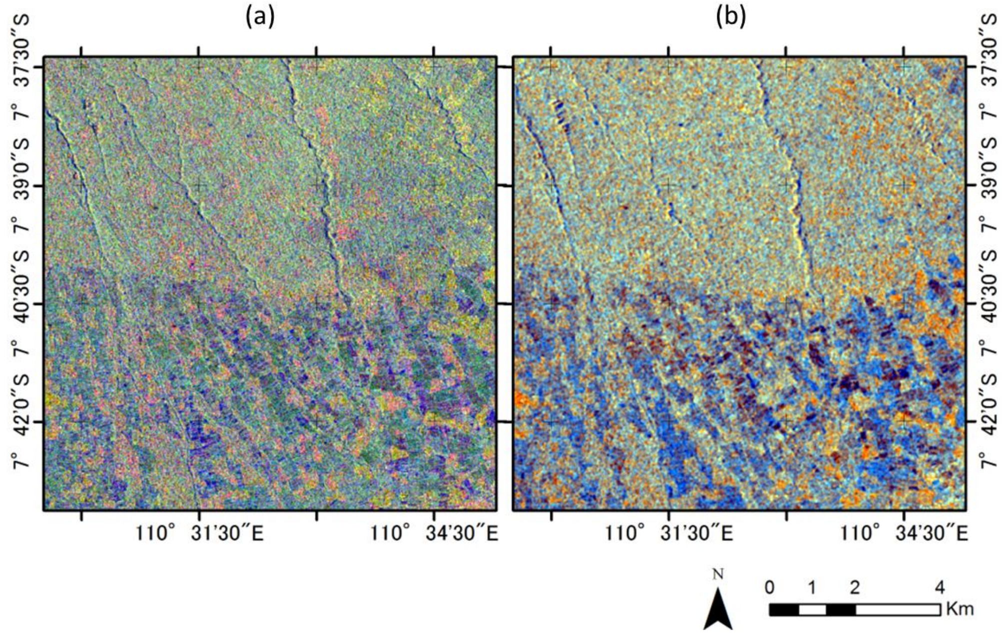

Figure 3: The Sentinel-1 image taken on 3 January 2017, (a) before speckle filtering process and (b) after speckle filtering process

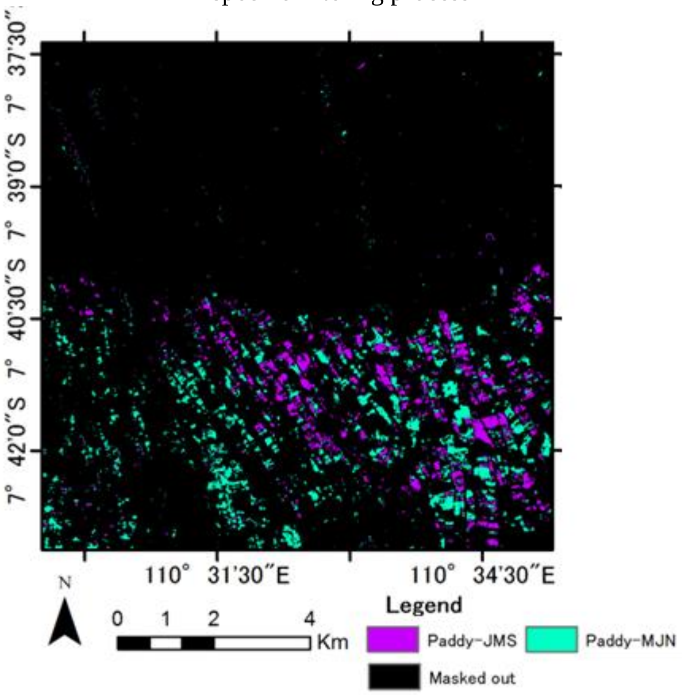

Figure 4: The distribution of Paddy-JMS and Paddy-MJN identification

In addition, the boundary between northern and southern area became clearer compared to the image before the speckle filtering process. The VV, VH, and VH-VV polarizations band composite follows (Cazals et al., 2016). In (Cazals et al., 2016) study shown that the VV, VH, and VH-VV polarization band composite capable to differentiate the flooded area with non-flooded area. In Figure 3(b), the dark blue color shows low backscatter coefficient and indicates areas with higher moisture conditions, such as from land irrigation or agricultural activities for paddy field cultivation. The cloud cover in Sentinel-2 can be eliminated by the cloud removal method. However, pixel value content similar to spectral value characteristics were identified as clouds or shadows and masked out in this process. The shadow removal is more difficult than the cloud cover removal due to its similarity with the water area and dense vegetation. Even though there is no large water body in the study area, the shadow can still be found in some part of the study area. Due to the high percentage of cloud coverage in several Sentinel-2 images, the Sentinel-2 was reduced from 49 images to 20 images.

3.2 Paddy Fields Area Identification

The pixel area coverage of Paddy-JMS and Paddy-MJN were calculated in GEE. The total area identified as Paddy-JMS and Paddy-MJN is approximately 415.83 Hectare and 548.78 Hectare, respectively. Figure 4 shows the area identified as Paddy-JMS in magenta and Paddy-MJN in cyan. The majority of paddy fields are identified in the southern part of study area. However, some bare or open fields in the northern part are also identified as Paddy-JMS or Paddy-MJN. These areas often inundated during rainfall and cause the moisture conditions to be higher than their surroundings. The backscatter coefficient became low which was misidentified as paddy fields.

The average of temporal backscatter coefficient and NDVI from Paddy-JMS and Paddy-MJN areas were calculated in GEE, which are shown in Figure 5. After cloud removal, there are five days that the Sentinel-1 and Sentinel-2 acquired the same satellite image: June 8, July 18, August 7, October 6, and December 5.

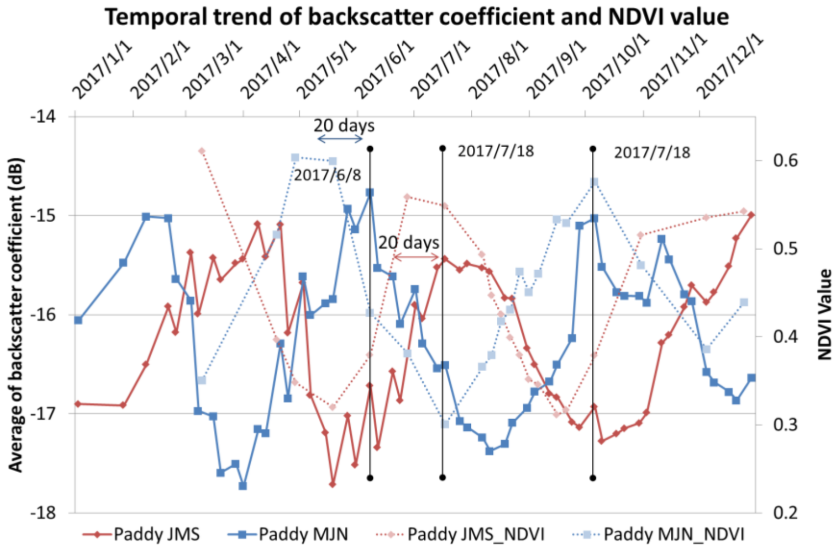

Figure 5: The average of VH polarization backscatter coefficient and NDVI value from paddy JMS and paddy

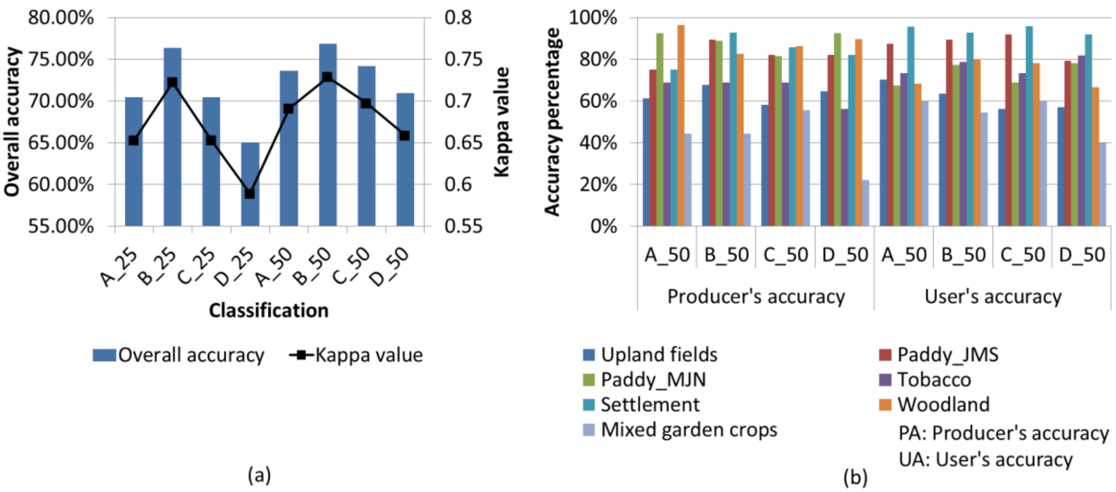

Figure 6: (a) The overall accuracy and kappa value of classification result and (b) the producer's and user's accuracy of all classes from random forest 50 classification

In order to simplify the visual presentation of the graph in Figure 5, only three dates were marked in black vertical lines. In general, the backscatter coefficient and NDVI value have similar temporal patterns. The fluctuating patterns of the backscatter coefficient in Figure 5 of Paddy-JMS occur from May to July. This phenomenon occurred because the Sentinel-1 images have two types of orbit modes—ascending and descending—that have different backscatter coefficients. The area identified as paddy fields has a low backscatter coefficient and NDVI value at the starting time of paddy cultivation for both cropping patterns. The low backscatter coefficient was influenced by the structure of the paddy growing stages. The backscatter coefficient is low during the preparation of paddy field cultivation. For the Paddy-JMS, cultivation occurs in January, from May to June, and from September to October. The backscatter coefficient increases until the mature stage and then starts to decrease near harvest time. The similar backscatter coefficients characteristic shows by the paddy cultivated in March, July and November.

However, the changes in backscatter coefficient trends came later compared to the NDVI value trend at around 20 days, which is the peak of the NDVI value in May for the Paddy-MJN, and the peak of the NDVI value in June for the Paddy-JMS. The NDVI value was derived from the optical remote sensing, meaning it is more sensitive to the greenness of the surface object. In comparison, the backscatter coefficient is more sensitive to surface structures conditions. As pointed by (Yang et al., 2008), the paddy growth parameters such as plant height, water content and plant structure are the most responsible for backscatter coefficient. Therefore, the backscatter coefficient remained high because the area was covered by the mature stage of paddy field, and the NDVI started to have a lower value because the greenness of paddy was fading. By contrast, the backscatter coefficient started to decrease, similar to NDVI value, immediately after the mature stage of paddy fields.

3.3 Classification Result

Random forest with 50 trees gave higher classification accuracy with an average above 70% than the random forest with 25 trees, as can be seen in Figure 6(a). The highest classification accuracy was obtained using a combination B_50, with 76.88% of the overall accuracy and 0.728 of the kappa value. The classification of D_25 gave the lowest accuracy, with 65.05% and 0.588 for overall accuracy and the kappa value, respectively. These results present that the additional bands from the subtraction of VH and VV polarizations increased both the overall accuracy and the kappa value, as can be seen in high accuracy for the classification of the B_25 and B_50 polarization band combination.

Amongst all classes, both of producer's and user's accuracy of mixed garden crops classes remained below 60%. The average accuracy of the mixed garden crops class from 8 classifications is 35.18% and 46.61%, for the producer's and the user's accuracy, respectively. The Figure 6(b) shows the producer's and user's accuracy classifications using random forest with 50 trees. The mixed garden crops class was often misclassified as an upland field class and a woodland class. The location of mixed garden crops is near the upland fields and is similar to upland fields but covered with tree canopy. It is because the C-band used for Sentinel-1 could not penetrate the dense canopy and received only the backscatter of the surface canopy. In the previous study (Mirelva and Nagasawa, 2018), mixed garden crops could be identified and classified better in L-band SAR, because the L-band could penetrate the canopy. Therefore, the mixed garden crops class tended to have lower accuracy and was misclassified as woodland class in C-band Sentinel-1. Settlement and woodland class have a minimum temporal change which influenced the stability of the backscatter coefficient in their surface area. Therefore, the accuracy of both classes is higher than other agricultural classes. The Paddy-JMS and Paddy-MJN have an acceptable producer's and user's accuracy above 65% for all classifications.

In Figure 7, the experimental part of study area sized 4 km^2 of land uses and land covers consisting of settlements, paddy fields, and tobacco fields, which was selected to evaluate the classification results. The Sentinel-2 was taken on May 19, 2017, with band 4, band 3, and band 2 as RGB composite image. Some areas of the Paddy-JMS and the Paddy-MJN class were misclassified as tobacco fields because the tobacco fields were planted in the paddy field area during the dry season. The visual interpretation of Sentinel-2 indicates that the plantation of tobacco fields started in the middle of May 2017 and finished around the end of September 2017. As a result, the net cover for tobacco plantation was removed and the area became paddy fields in October. Therefore, the tobacco fields were correctly identified in A_50, B_50, and C_50. However, in D_50, some areas, which were identified with a yellow circle, were classified as the paddy fields and upland fields because the fields were cultivated after harvesting the tobacco fields. Figure 8 shows the average of VH polarization backscatter coefficient for all classes.

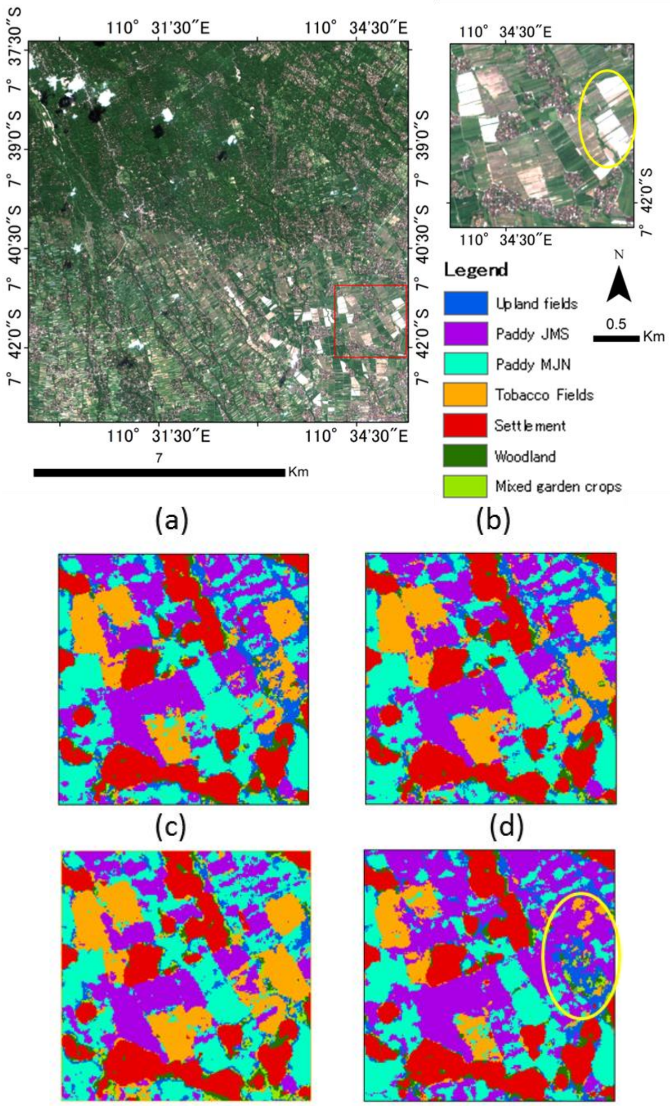

Figure 7: The image of Sentinel-2 taken on 19 May 2017 and classification result for (a) A_50, (b) B_50, (c) C_50 and (d) D_50 with experimental part shows in red square

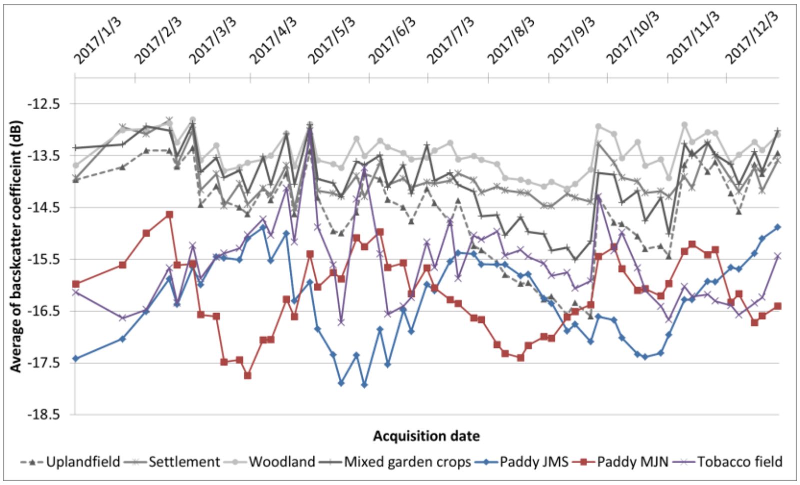

Figure 8: The average of VH polarization backscatter coefficient for all classes

The backscatter coefficient of tobacco fields is relatively low, around -16 dB during wet season in January and December after the harvest of tobacco field. Therefore, the tobacco fields were often misclassified as paddy fields. The other classes, such as woodland and settlement, have the most stable VH polarization. In this study, the complex agricultural area and two paddy fields cropping pattern can be identified and classified using Sentinel-1 in GEE. In VH polarization, the Paddy-JMS, the Paddy-MJN, and the tobacco fields class have a lower average backscatter coefficient than other classes. A study conducted by (Tian et al., 2018) confirmed that the backscatter coefficient of paddy fields was lower than the backscatter coefficient of other land covers. The backscatter coefficient of tobacco fields reached the highest backscatter coefficient on May 3, 2017, and May 30, 2017, which are almost equal to other classes, such as woodland, settlement, upland fields, and mixed garden crops. The low moisture from land preparation for tobacco fields affected the low moisture in the soil, which shows in high backscatter coefficient.

4. Conclusion

The temporal microwave satellite images, such as Sentinel-1, could contain a large amount of data, and require a lot of storage for processing. However, GEE provides cloud-based storage for processing satellite images, including Sentinel-1. In this study, the Sentinel-1 data assisted with Sentinel-2 were successfully classified for the complex agricultural area in GEE platform. The threshold of backscatter coefficient less than -17.4852 dB and greater than -31 dB generated a paddy fields area. As a result, the cropping pattern of paddy fields was calculated based on how many times paddy fields were cultivated. In this study, the cropping patterns were separated into two types, Paddy-JMS (paddy planted in January, May, and September) and Paddy-MJN (paddy planted in March, July, and November). The average producer's and user's accuracy for both paddy fields was above 65%. A comparison of the backscatter coefficient and NDVI value of these paddy fields classes shows the backscatter coefficient was more sensitive to the surface structure, which led to the shifting time between the backscatter coefficient and NDVI. The random forest with 50 trees gave higher accuracy than the random forest with 25 trees, especially accuracy for the dataset with less polarization band combination. The combination band of VH, VV, and the subtraction of VH and VV polarization classified with the random forest with 50 number of trees obtained the highest overall accuracy and kappa value as 76.88% and 0.728, respectively. In this study, the Sentinel-1 was found to be very useful for agricultural croplands, especially paddy fields with different cropping patterns. The Sentinel-2 provides NDVI and the images for selected sample points and accuracy assessment points. As a result, the processing of Sentinel-1 and Sentinel-2 using GEE could successfully be applied in the agricultural croplands classification in tropical areas.

References

Agus, F. and Manimkmas, M. O. A., 2003, Environmental Roles of Agriculture in Indonesia. *Presented at the 25th Conference of the International Association of Agricultural Economist, Durban, South Africa*. Retrieved from ftp://193.43.36.92/es/esa/roa/pdf/2_Environment/Environment _IndonesiaNA.pdf.

Breiman, L., 2001, Random Forests. *Machine Learning*, Vol. 45 (5), 5-32. https://doi.org/10.1023/A:1010933404324.

Cazals, C., Rapinel, S., Frison, P. L., Bonis, A., Mercier, G., Mallet, C., Corgne, S. and Rudant, J. P., 2016, Mapping and Characterization of Hydrological Dynamics in a Coastal Marsh Using High Temporal Tesolution Sentinel-1A Images. *Remote Sensing*, Vol. 8(7), 570. https://doi.org/10.3390/rs8070570.

Clauss, K., Ottinger, M. and Kuenzer, C., 2017, Mapping Rice Areas with Sentinel-1 Time Series and Superpixel Segmentation. *International Journal of Remote Sensing*, Vol. 39, No. 5, 1399-1420.

Ghazaryan, G., Dubovyk, O., Löw, F., Lavreniuk, M., Kolotii, A., Schellberg, J. and Kussul, N., 2018, A Rule-Based Approach for Crop Identification Using Multi-Temporal and Multi-Sensor Phenological Metrics. *European Journal of Remote Sensing*, Vol. 51(1), 511-524, DOI: 10.1080/22797254.2018.1455540.

Mirelva, P. R. and Nagaswa, R., 2018, Identification and Classification of Complex Agricultural Croplands Using Multi-Temporal ALOS-2/PALSAR-2 Data: A Case Study in Central Java, Indonesia. *Journal of Agricultural Science*, Vol. 10(2), 58-70.https://doi.org/10.5539/jas.v-10n2p58.

Nelson, A., Setiyono, T., Rala, A. B., Quicho, E. D., Raviz, J. V., Abonete, P. J., Maunahan, A. A., Garcia, C. A., Bhatti, H. Z. M., Villano, L. S., Thongbai, P., Holecz, F., Barbieri, M., Collivignarelli, F., Gatti, L., Quilang, E. J. P., Mabalay, M. R. O., Mabalot, P. E., Barroga, M. I., Bacong, A. P., Detoito, N. T., Berja, G. B., Varquez, F., Wahyunto, Kuntjoro, D., Murdiyati,

S. R., Pazhanivelan, S., Kannan, P., Mary, P. C. N., Subramanian, E., Rakwatin, P., Intrman, A., Setapayak, T., Lertna, S., Minh, V. Q., Tuan, V. Q., Duong, T. H., Quyen, N. H., Van Kham, D., Hin, S., Veasna, T., Yadav, M. , Chin, C. and Ninh, N. H., 2014, Towards an Operational SAR-Based Rice Monitoring System in Asia: Examples from 13 Demonstration Sites across Asia in the RIICE Project. *Remote Sensing*, Vol. 6(11), 10773-10812.

Parmes, E., Rauste, Y., Molinier, M., Andersson, K. and Seitsonen, L., 2017, Automatic Cloud and Shadow Detection in Optical Satellite Imagery Without Using Thermal Bands—Application to Suomi NPP VIIRS Images over Fennoscandia. *Remote Sensing*, Vol. 9(8), 806; doi:10.3390/rs9080806.

Saxena, N. and Rathore, N., 2013, A Review on Speckle Noise Filtering Techniques for SAR Images. *International Journal of Advanced Research in Computer Science and Electrnoic Engineering(IJARCSEE)*, Vol. 2(2), 243-247.

Shelesto, A., Lavreniuk, M., Kussul, N., Novikov, A. and Skakun, S., 2017, Exploring Google Earth Engine Platform for Big Data Processing: Classification of Multi-Temporal Satellite Imagery for Crop Mapping. *Frontiers in Earth Science*, Vol. 5, https://doi.org/10.3389/feart-.2017.00017.

Sidhu, N., Pebesma, E. and Câmara, G., 2018, Using Google Earth Engine to Detect Land Cover Change: Singapore as a Use Case, E*uropean Journal of Remote Sensing*, Vol. 51(1), 486-500, DOI: 10.1080/22797254.2018.-1451782.

SNAP Software, Brockmann Consult, Array Systems Computing and C-S. Available online: http://www.step.esa.int/main/toolboxes/snap/ (Last accessed on 10 April 2019).

Tian, H., Wu, M., Wang, L. and Niu, Z., 2018, Mapping Early, Middle and Late Rice Extent Using Sentinel-1A and Landsat-8 Data in the Poyang Lake Plain, China. *Sensors,* Vol. 18(1), https://doi.org/10.3390/s18010185

Torbick, N., Diya, C., Salas, W. and Qi, J., 2017, Monitoring Rice Agriculture Across Myanmar Using Time Series Sentinel-1 Assisted by Landsat-8 and PALSAR-2. *Remote Sensing*. Vol. 9(2), 119, https://doi.org/10.3390/rs90-20119

Veloso, A., Mermoz, S., Bouvet, A., Toan, T. L., Planells, M., Dejoux, J. F. and Ceschia, E., 2017, Understanding the Temporal Behavior of Crops Using Sentinel-1 and Sentinel-2-like Data for Agricultural Applications. *Remote Sensing of Environment*, Vol. 199, 415–426.

Xiong, J., Thenkabail, P. S., Gumma, M. K., Teluguntla, P., Poehnelt, J., Congalton, R. G., Yadav, K. and Thau, D., 2017, Automated Cropland Mapping of Continental Africa Using Google Earth Engine Cloud Computing. *ISPRS Journal of Photogrammetry and Remote Sensing.* Vol. 126, 225-244, https://doi.org/10-.1016/j.isprsjprs.2017.01.019.

Yang, S., Shen, S., Li, B., Le Toan, T. and He, W., 2008, Rice Mapping and Monitoring Using ENVISAT ASAR Data. *IEEE Geoscience and Remote Sensing Letters,* Vol. 5(1), 108-112, https://doi:10.1109/lgrs.2007.912089

Yusoff, N. M., Muharam, F. M., Takeuchi, W., Darmawan, S. and Razak, M. H. A., 2016, Phenology and Classification of Abandoned Land Based on ALOS-1 and 2 PALSAR Multi-Temporal Measurements. *International Journal of Digital Earth*, Vol. 10(2), 155-174. https://doi.org/10.1080/17538947.2016.1216615.

Zhang, Y., Wang, C. and Zhang, Q., (2011). Identifying paddy fields with dual-polarization ALOS/PALSAR data. Canadian Journal Remote Sensing, Vol. 37(1), pp. 103-111.